Ankle Exoskeletons May Hinder Standing Balance in Simple Models of Older and Younger Adults

Daphna Raz, *Student Member, IEEE*, Varun Joshi, Brian R. Umberger, and Necmiye Ozay *Senior Member, IEEE*

***Abstract*— Humans rely on ankle torque to maintain standing balance, particularly in the presence of small to moderate perturbations. Reductions in maximum torque (MT) production and maximum rate of torque development (MRTD) occur at the ankle with age, diminishing stability. Ankle exoskeletons are powered orthotic devices that may assist older adults by compensating for reduced muscle force and power production capabilities. They may also be able to assist with ankle strategies used for balance. However, no studies have investigated the effect of such devices on balance in older adults. Here, we model the effect ankle exoskeletons have on stability in physics-based models of healthy young and old adults, focusing on the mitigation of age-related deficits such as reduced MT and MRTD. We show that an ankle exoskeleton moderately reduces feasible stability boundaries in users who have full ankle strength. For individuals with age-related deficits, there is a trade-off. While exoskeletons augment stability in low velocity conditions, they reduce stability in some high velocity conditions. Our results suggest that well-established control strategies must still be experimentally validated in older adults.**

***Index Terms*— Aging, biomechanics, exoskeletons, human stability, standing balance.**

I. Introduction

Ankle exoskeletons are powered orthotic devices that can assist people with mobility impairments, such as older adults, by compensating for reduced muscle force and power capabilities. Typically, they provide actuation about the ankle joint only in the sagittal plane, generating a push-off torque during dynamic activities such as walking and stair climbing. Exoskeletons have been shown to reduce metabolic cost of transport during walking, in both younger [1] and older adults [2]. The main source of their appeal to older adults, however, is their perceived potential to reduce fall risk [3]. It is therefore crucial to develop our understanding of the effect of ankle exoskeleton assistance on stability, which is currently incomplete.

Torque production at the ankle is an important contributor to balance, which suggests that ankle exoskeletons have the potential to improve stability during standing. Unimpaired adults tend to rely on ankle torques to maintain a stable standing position, only switching to a hip strategy in response to large perturbations [4]. In older adults, maximum available plantar flexion and dorsiflexion torques are lower, reducing the range of perturbations that can be accommodated with an ankle strategy [5]. This reduction in peak ankle torque has been shown in multiple studies to be correlated with decreased performance in balancing tasks [5] and a higher risk of falls [6], [7]. The rate at which this torque can be produced also declines with age [8], although the effect of a lower maximum rate of torque development (MRTD) on standing balance is inconclusive. Reduced MRTD at the knee is associated with a history of falls [9], [10], while plantar flexor MRTD is significantly correlated with lower performance on a single standing leg balance test for older men, but not for older women [11]. Other studies have found that lower ankle MRTD is not a strong predictor of fall likelihood [12], [13]. Still, it is possible that lower MRTD contributes, independently of lower MT, to increased fall risk in older adults.

Although ankle exoskeletons can, in theory, mitigate both MT and MRTD deficits by producing large amounts of torque quickly, the effect they have on stability is unclear. Depending on the population, device, controller, and perturbation paradigm, ankle exoskeletons have been reported to enhance stability [14]–[16], slightly reduce stability [15], [17], or have no effects on stability [18], [19]. Notably, the majority of balance studies for powered exoskeletons have focused on young and able bodied users, who do not have impaired stability. As these devices are likely to be marketed to enhance mobility in older populations [3], it is imperative to understand how these they may affect the stability of users with age-related reduction in MT and MRTD. We currently do not know how these age-related changes may interact with additional exoskeleton assistance at the ankle. Because perturbation experiments on older adults are expensive, time-consuming, and risky, developing a generalizable model-based characterization of standing balance with ankle exoskeletons is a useful approach. Modeling can provide insights into the mechanisms underlying exoskeleton-assisted standing balance, including how constraints on the human-exoskeleton system are affected both by the device and by age-related joint-level torque deficits.

Bounds on human stability for feet-in-place activities such as standing may be characterized by computing the set of all body center of mass (CoM) positions and velocities from which it is possible to stabilize to quiet standing, meaning that the CoM position is above the foot and the CoM velocity is close to zero [20]. This set is sometimes called the feasible stability region [21], [22]. In the case of a simplified linear inverted pendulum these are the well-known extrapolated center of mass boundaries [23]. In this text we will use the term stabilizable region, abbreviated 'SR,' as in our previous work.

Stabilizable regions have been computed for various legged dynamical systems [24], [25], including one example where the boundary was partially computed for a model of a human wearing an optimally controlled hip-knee-ankle exoskeleton [26]. The full stabilizable region under aging-related biological constraints and different ankle exoskeleton controllers has not been explored. Furthermore, formal stability properties of this region have not been defined. One particularly important attribute is invariance. If the SR is controlled invariant, this means that there always exists a controller that allows the human to stay within the region. If it is not, then there may be states within this region from which the human can pass through the SR, but not stabilize. Invariance guarantees that the SR does not include states which merely pass through the set. This property is particularly important to verify when there are constraints on the control input. Such constraints may correspond to biologically meaningful quantities such as maximum joint torque, or to environmental constraints such as the frictional forces on the support surface.

In a previous paper, we introduced a general framework for determining the complete SR boundary for human-exoskeleton dy-

This work was supported by NIH grants F31-EB032745 and R01AG068102.

D. Raz and N. Ozay are with the University of Michigan Robotics Institute, Ann Arbor, MI USA (e-mail: daphraz@umich.edu, necmiye@umich.edu).

V. Joshi and B. R. Umberger are with the University of Michigan School of Kinesiology, Ann Arbor, MI USA (e-mail: varunjos@umich.edu, umberger@umich.edu).

namical systems [27]. Our approach formulates the SR boundary as the solution of a single partial differential equation rather than an algorithmic search. In contrast to prior work, we include strong formal invariance and stability guarantees over the entire SR in the presence of both biological and environmental constraints.

Here we provide a generalizable, model-based understanding of how an ankle exoskeleton may alter the domain of invariant stable motions available to a user in the presence of joint level functional changes associated with aging, including reduced MT production and MRTD. To our knowledge, this is the first study that attempts to systematically understand the combined effect of ankle exoskeleton assistance and age-related ankle torque deficits on feasible stability. Using common exoskeleton control strategies, we analyze the effect that exoskeletons have of the invariant stabilizable region for models of healthy young and healthy old adults. We show that while exoskeletons can indeed enhance ankle torque production and improve stability under certain conditions, they can also act as a disturbance, resulting in a trade-off between increased torque bounds and stability.

II. Preliminaries

Our methods for computing stabilizable regions (SRs) are based on two notions, controlled invariance and backward reachability, which we formally define in the following sections.

A. Controlled invariance and backward reachability

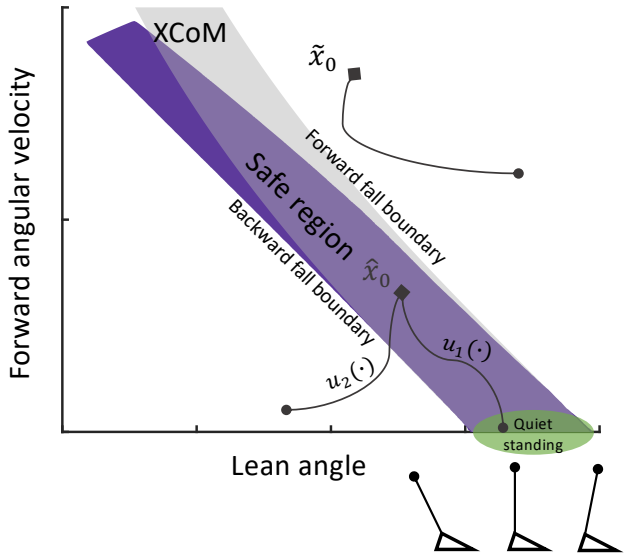

Fig. 1. Illustration of a target set (green) and its backward reachable set (purple). The state $\hat{\boldsymbol{x}}_0$ is in the BRS because there exists a controller $\boldsymbol{u_1}$ that drives the system to the target set at time $\boldsymbol{T}$. No such controller exists for $\tilde{\boldsymbol{x}}_0$ so it is not in the BRS. Note that controller $\boldsymbol{u_2}$ does not drive the system to the target. If the target set is controlled invariant then the union of the target set and the BRS is also invariant. Here, the BRS was computed with model parameters corresponding to a young male, using our method described in Section IV. The gray region is computed using the extrapolated center of mass (XCoM) method from [23], which we have converted here to angular coordinates.

Consider the system

$$\dot{x} = f(x, u), \tag{1}$$

where state $x \in X \subset \mathbb{R}^n$, input $u \in U \subset \mathbb{R}^m$. Control signals are denoted $u(\cdot) \in \mathcal{U} = \{\phi : [0, \infty] \to U\}$. Solutions to this system are functions of time, and we denote them by $\varphi(\cdot; x_0, u(\cdot))$, for initial condition x_0 and control signal $u(\cdot)$.

A set $\Omega \subset X$ is controlled invariant if for any initial condition in the set, there exists a controller that maintains the system state within Ω:

Definition 1. A set $\Omega \subset X$ is *controlled invariant* for system (1) if, for all $x_0 \in \Omega$, there exists $u(\cdot) \in \mathcal{U}$ such that for all $t \in [0, \infty]$, $\varphi(t; x_0, u(\cdot)) \in \Omega$.

If Ω is a safe region in the state space, then the ability to always stay within the set is a desirable property.

We can also define the region of the state space from which it is possible to reach a specified (not necessarily invariant) subset, S. The set of all $x \in X$ such that there exists a control signal that drives the system to S within some finite time horizon is the backward reachable set of S.

Definition 2. Let $S \subset X$ and $T \in \mathbb{R}_0^+$. Then $\mathcal{G}_T(S)$, the *backward reachable set* of S at time T, is

$$\mathcal{G}_T(S) := \{x \in X \mid \exists u(\cdot) \in \mathcal{U} \, s.t. \, \varphi(T; x, u) \in S\}. \tag{2}$$

An illustration of this set is depicted in Figure 1. Because this definition does not constrain the form of the control law, it is the *maximal* backward reachable set (BRS) with respect to $\mathcal{U}$. Thus it represents the 'best case' scenario of the states from which it is possible to reach the target set.

The BRS only contains states from which the system can reach the target set at precisely time T. The set of all states from which the target set can be reached at $t \leq T$ is called the backward reachable tube, and is a union of backward reachable sets:

Definition 3. The *maximal backward reachable tube* of a set $S \subset X$ over a time horizon $[0, T]$ is $\mathcal{G}_{[0,T]}(S) = \cup_{t \in [0,T]} \mathcal{G}_t(S)$.

Given these definitions, we note the following two facts:

Fact 1. *If Ω is controlled invariant, then its backward reachable set is controlled invariant.*

Fact 2. *Assume a system as defined in* (1)*. Let $S \subset X$ be controlled invariant. Then $\mathcal{G}_{t_1}(S) \subset \mathcal{G}_{t_2}(S)$ for all t_1, $t_2 \in \mathbb{R}^+$ with $t_1 < t_2$.*

Fact 2 is proved in [27]. Taken together, these facts mean that for an invariant target set S, $G_{[0,T]}(S) = G_T(S)$. Thus it is sufficient to compute the backward reachable set rather than computing the full reachable tube.

B. Relating invariance and reachability to human stability

The relationship between human stability and our formal mathematical definitions is illustrated in Figure 1. Assume that the dynamics (1) represent a parameterized model of a standing human. In the figure, the green ellipse represents a controlled invariant target set of states corresponding to quiet standing. Note that for the purposes of the illustration the set is depicted to be larger than it is. The purple region is the true-to-size backward reachable set that we compute using a constrained dynamical model with parameters corresponding to a young male, as described later in Section III. As labeled in the figure, the boundaries of this set correspond to forward and backward fall boundaries and to constraint failures. Outside of these boundaries the ankle strategy fails and the model must take some action to avoid a fall, such as taking a step. For visual clarity we only depict the portion of the state space corresponding to forward angular velocities. Because the target set is controlled invariant, the resulting purple safe region is as well. For comparison, we show the same bounds computed using the extrapolated center of mass method, from [23], in light gray.

To determine the stability bounds of the human-exoskeleton system, we also compute reachable sets with the dynamics of an ankle

exoskeleton controller added to (1), the details of which are presented in Section III and IV. We construct invariant target sets corresponding to quiet standing with exoskeleton assistance, and then compute the backward reachable sets. The resulting sets then delineate the feasible stabilizable boundaries with ankle exoskeleton assistance.

III. Human-Exoskeleton Model

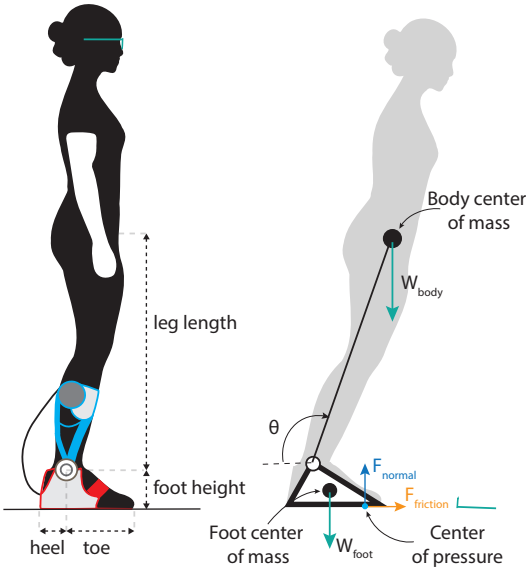

Fig. 2. Free body diagram representing the forces acting on the combined human-exoskeleton system.

We use a planar, two link, single degree-of-freedom model to represent a standing human (Fig 2). The first link represents the foot, while the second link represents the rest of the body. These links are connected using a pin-joint at the ankle, with the axis of rotation lying normal to the sagittal plane. The mass of each link is assumed to be lumped at the center-of-mass for the respective body. The human interacts with the ground through forces applied on the foot segment. Thus, these ground reaction forces applied at the foot, and the weight of the foot and body segments applied at each respective mass center, are the only external forces acting on the human system.

We model the ankle exoskeleton as massless device, worn bilaterally, that only generates torque in the sagittal plane. We assume that the the human can resist the torque generated by the device if necessary. Thus the exoskeleton is represented by an ideal torque actuator at the ankle, and the net torque at the ankle is the sum of the human and the exoskeleton torques.

Rather than including the human torque τ_{human} as an ideal (instantaneous) torque actuator, we use a more realistic simplified actuation model where the direct human input to the system is the desired rate of torque development, $\dot{\tau}^{\text{des}}_{\text{human}}$. The stabilizable configurations are thus represented in joint angle-velocity-torque space, where the torque state represents the human torque only. Denoting the state space as $X \subset \mathbb{R}^3$, with $x_1 = \theta, x_2 = \dot{\theta}$ and $x_3 = \tau_{\text{human}}$, and the input space as $U \subset \mathbb{R}$ with input $u = \dot{\tau}^{\text{des}}_{\text{human}}$, in state space form, our dynamics are

$$\begin{bmatrix} \dot{x}_1 \\ \dot{x}_2 \\ \dot{x}_3 \end{bmatrix} = \begin{bmatrix} x_2 \\ -\frac{g}{l}\cos x_1 - \frac{b}{ml^2}x_2 + \frac{1}{ml^2}(x_3 + \tau_{\text{exo}}) \\ u \end{bmatrix}. \quad (3)$$

The constants g, m, and l represent the gravitational acceleration, mass of the body link, and leg length. The parameter b represents minimal damping that is included make the dynamics less stiff.

We can thus limit the torque that the human can produce (MT) and the maximum rate of torque change (MRTD) of the model by constraining state x_3 and input u:

$$\tau^{\text{max pf}}_{\text{human}} \leq x_3 \leq \tau^{\text{max df}}_{\text{human}} \quad (C1)$$

$$\text{MRTD}^{\text{max pf}} \leq u \leq \text{MRTD}^{\text{max df}} \quad (C2)$$

Maximum plantar flexion torque $\tau^{\text{max pf}}_{\text{human}}$ is negative in our angle convention, while $\tau^{\text{max df}}_{\text{human}}$ denotes positive dorsiflexion torque. Lower magnitude of torque bounds correspond to weaker ankle strength, while lower bounds on u correspond to reduced rate of torque development, as seen in older adults [8].

As, shown in Figure 2, the foot contact with the ground is determined by the normal force F_{normal}, the force due to friction F_{friction} with coefficient of static friction μ, and the location of the center of pressure (CoP). The CoP should remain within the base of support (BoS), which corresponds to the length of the foot. Full ground contact is enforced by three zero-moment point (ZMP) safety constraints which prevent the foot from tipping or slipping [28]:

$$F_{\text{normal}} \geq 0 \quad (C3)$$

$$\text{CoP} \in \text{BoS}, \quad (C4)$$

$$|F_{\text{friction}}| < \mu F_{\text{normal}}. \quad (C5)$$

A human user may respond to the assistive torque of the exoskeleton in a range of ways. They may actively resist the torque generated by the device, or they may adapt their torque production to allow the exoskeleton to assist as much as possible. Studies with able-bodied participants, such as [19] have shown that young adults adapt quickly to an exoskeleton using a state-feedback controller, with minimal alteration to CoM kinematics. Thus we make the following assumptions related to the human-exoskeleton interaction:

1) The exoskeleton employs a state feedback control strategy and is unaware of the foot-ground interaction constraints-cannot reduce or increase torque production if a foot-ground interaction constraint is in danger of being violated
2) The human increases or decreases their torque production to account for the torque produced by the exoskeleton, in an effort to be optimally safe
3) The human cannot instantaneously change the value of the torque produced at the ankle

Assumption 3 is addressed via constraint (C2). Because of Assumption 2, (C3)-(C5) can be expressed as constraints on the total torque of the system such that the exoskeleton torque is accounted for. Let $h : X \to \mathbb{R}$. Then we can write constraints on the torque as:

$$h^k_{\text{lb}}(x) < x_3 + \tau_{\text{exo}}(x) < h^k_{\text{ub}}(x) \quad (4)$$

for $k \in \{1, 2, 3\}$. As we assume the exoskeleton torque is a function of state, these are actually state constraints on the human torque state x_3. Appendix I includes a full derivation of the equations of motion and foot-ground contact constraints.

IV. Methods

We assess the effect of ankle exoskeletons on feasible stability by computing the BRS of the human-exo system for two exoskeleton controllers, over a range of sex- and age-adjusted model parameters.

A. HJB Reachability

The BRS can be computed using Hamilton Jacobi reachability tools. Hamilton Jacobi Bellman reachability uses HJB partial differential equations to compute implicit set representations of the backward reachable set [29]. We provide a brief overview of the method here, but we note that our analysis can be done with any nonlinear continuous time backward reachability tool. A more rigorous development of HJB and its use for solving reachability problems can be found in [30].

Given a dynamical system of the form (1) and a target set $S \subset X$, let $g(x)$ be a function whose zero sublevel set represents S, i.e., $S = \{x \mid g(x) \leq 0\}$. Typically $g(x)$ is a signed distance function. HJB reachability tools compute the backward reachable set by solving the PDE

$$D_t V(t,x) + H(t,x,\nabla V) = 0,\ V(0,x) = g(x). \tag{5}$$

over reversed time interval $[-T, 0]$, where T is the desired duration and $t \in [-T, 0]$. The solution $V(t,x)$ is called the value function. The function $H(t,x,\nabla V)$ is called the Hamiltonian, and in this case is given by

$$H(t,x,\nabla V) = \min_{u \in U} \nabla V \cdot f(x,u) \tag{6}$$

The argument of the Hamiltonian,

$$a^*(x) \in \arg\min_{u \in U} \nabla V \cdot f(x,u) \tag{7}$$

is an optimal control input at a given state x that minimizes $V(x,t)$ along the system trajectory. The value function itself is an implicit surface function representation of the backward reachable set at time t, $\mathcal{G}_t$, as defined in Definition 2. Thus,

$$\mathcal{G}_t = \{x \mid V(t,x) \leq 0\}. \tag{8}$$

Note that we abuse notation slightly by letting t also denote $t \in [0, T]$ in the nonreversed time interval.

Suppose now that system (1) is control affine, such that it can be written

$$\dot{x} = f(x,u) = f^x(x) + f^u(x)u. \tag{9}$$

We assume that $u \in U \subset \mathbb{R}^m$ and that U is a hyperrectangle such that u is bounded elementwise, i.e. $u_i \in [\underline{u_i}, \overline{u_i}]$. In this case, an analytical solution to Problem (7) is quite easy to find. As the optimization is over u, portions of the resulting expression that do not contain the control input can be ignored, and the problem reduces to

$$a^* \in \arg\min_{u \in U} \sum_{i=1}^{n} \frac{\partial V(t,x)}{\partial x_i} f_i^u(x) \cdot u_i \tag{10}$$

The optimization problem is evaluated at a fixed time t and state x, which means that each coefficient $\frac{\partial V(t,x)}{\partial x_i} \cdot f_i^u(x)$ is a constant. The solution can thus be found easily by letting $u_i = \underline{u_i}$ if the coefficient is positive and $u_i = \overline{u_i}$ otherwise. For system (3), equation (10) reduces to

$$\min_{u \in U} H(t,x,\nabla V) = \frac{\partial V(x,t)}{\partial x_3} u. \tag{11}$$

Assuming $U = [\underline{u}, \overline{u}]$, the optimal controller is therefore $\overline{u}$ if coefficient $\frac{\partial V(x,t)}{\partial x_3} < 0$ and $\underline{u}$ otherwise.

B. Constructing invariant target sets

Recall that controlled invariance is a desirable safety property. To ensure that the BRS is controlled invariant, it suffices to show that the target set is controlled invariant, as explained in Section II. However, in our case, the target set must be a subset of the safe region defined by constraints (C1) and (C3)-(C5), and obey constraints on the controller (C2). Thus the target sets must be constructed with care.

Appropriate candidates for the target set can be found in the biomechanics literature, where feasible stability is commonly defined as the ability to reach static standing configurations [20]. These are equilibrium configurations where (i) the angular velocity of the body is zero and (ii) the x-coordinate of the center of mass (CoM_x) is within the base of support (i.e. above the foot). These configurations form a continuum that can be used to construct target sets.

We show this by first analyzing static equilibrium (zero net-torque) states that fulfill condition (i). Let τ_{act} denote the total actuation torque about the ankle, as in Figure 2, and let $\tau_g = mgl\cos\theta$ be the gravitational torque. Summing the torques, we see that $\tau_{\text{act}} = \tau_g$ meaning that the net actuation torque must remain constant and compensate for gravity. With human torque τ_{human} state feedback exoskeleton torque τ_{exo}, we have that $\tau_{\text{act}} = \tau_{\text{human}} + \tau_{\text{exo}}$. Also recall that in our 'lifted' system (3), input $u = \dot{\tau}_{\text{human}}$, is the rate of the human torque development. Therefore we have that at equilibrium, $\tau_{\text{human}} = \tau_g - \tau_{\text{exo}}$ and $u = 0$.

There are multiple static equilibria corresponding to various resting states where the net actuation torque counters gravity, which can be defined as the following set

$$\Omega_{eq} = \{x \in X | x_2 = 0, x_3 = \tau_g - \tau_{\text{exo}}\}. \tag{12}$$

Curves representing these equilibria for system (3) with and without an exoskeleton are shown in Figure 3. The depicted exoskeleton controller, which is described in more detail in the following sections, compensates for gravity and saturates at $50\,\text{N}\cdot\text{m}$.

Our desired static equilibria must also satisfy condition (ii), with the CoM_x above the foot. In angular coordinates, the bounds of the foot can be represented as the maximum forward and backward lean angle, such that the CoM_x is within the foot. We refer to the maximum forward lean as θ_{toe} and the backward lean angle as θ_{heel}. Using the geometric parameters of the foot as shown in Figure 2, we have that $\theta_{\text{heel}} = \cos^{-1}\left(\frac{a}{l}\right)$ and $\theta_{\text{toe}} = \cos^{-1}\left(\frac{l_f - a}{l}\right)$. This gives a feasible range of lean angles, $\theta \in [\theta_{\text{heel}}, \theta_{\text{toe}}]$.

To model humans realistically, we also account for limits on τ_h shown in constraint (C1). The feasible target states consist of the intersection of the set of states where the constraints on joint angle are satisfied and the set where the constraints on torque production are satisfied. These are shown inside the green square in Figure 3. Note that all static equilibria within this square also satisfy constraints (C3)-(C5). This is because at these states, the system is not accelerating and is at zero velocity - therefore the ground reaction force is equal to the weight of the foot and body, there is no friction force, and the CoP is within the bounds of the foot. Thus we have a continuum of goal positions within the safe region, where the foot maintains contact with the ground without tipping or slipping.

This representation of the target set raises two key concerns. First, because the set consists only of static equilibria, it does not allow for natural postural sway, which is a fundamental characteristic quiet standing in humans. Secondly, one-dimensional target sets consisting of curves or line segments can lead to computational issues when computing the BRS. To generate target sets that are more biologically realistic, we instead use a Control Lyapunov Function (CLF) to construct controlled invariant ellipsoids. CLFs are an extension of Lyapunov functions to systems with control, and are defined as follows [31]:

Definition 4. Let $x^* = 0$ be an equilibrium point of (1) and let $E : \mathbb{R}^n \to \mathbb{R}$ be a positive-definite, continuously differentiable and radially unbounded function. Then $E(\cdot)$ is a *control Lyapunov*

function if for all $x \neq 0$ there exists u such that $\dot{E}(x,u) < 0$.

In other words, a control input exists that stabilizes the system at x^*. Note that just as the level sets of Lyapunov functions are invariant, the level sets of a CLF are also controlled invariant. The level sets of an appropriately formulated CLF can therefore be used as target sets.

We start by first selecting the relevant equilibrium points. Due to computational scaling issues we compute the backward reachable sets in the space of positive (posterior to anterior) and negative (anterior to posterior) velocities separately. Segmenting the state space in this manner means that the backward reachable sets may not include initial conditions whose resulting trajectories oscillate between (large) positive and negative velocities while satisfying the constraints. To mitigate this issue within reasonable bounds for human balance, we include a buffer within our velocity range such that we compute over $[v_{\text{buffer}}^-, v_{\text{lb}}^+]$. We select the size of this buffer to be $0.5\,\text{rad}\,\text{s}^{-1}$, which is the largest computationally feasible bound. Our backwards reachable sets therefore exclude true failure states — from which it is impossible to reach the target set, and high oscillation states — from which it is only possible to reach the target set with oscillations of a magnitude higher than v_{buffer}. We note that in practice the size of the velocity buffer does not affect the resulting BRS and it is likely that highly oscillatory solutions do not satisfy constraints.

Because we compute the BRS in two separate forward and backward velocity segments, the target set formulation must encompass all the portions of the foot that we wish to reach with mostly positive and mostly negative velocity only. We therefore make the following observation: If an equilibrium point near the toe can be reached with a positive velocity, then any point posterior to that can be eventually reached with a low enough negative velocity, i.e. by leaning back slowly. This implies that it is sufficient to select one equilibrium point at the toe, rather than having to represent the entire range of static equilibria. A symmetric argument can be made for an equilibrium point at the heel or ankle for points that can be reached with a negative velocity. However, when the system includes a saturating exoskeleton torque due to the device's motor limits, the dynamics become hybrid. There are three modes corresponding to 1) negative saturation, 2) no saturation, and 3) positive saturation. These modes can be seen in Figure 3. Only two modes appear within the green region. Thus we will select one equilibrium point per mode: a 'toe' equilibrium point in mode 1, and an 'ankle' equilibrium point in mode 2.

To select the equilibrium point at the toe, we must take into account the functional base of support (FBOS). An individual's FBOS is defined as the maximum range that they can voluntarily translate their CoP in the anterior (toward the toe) and posterior (toward the heel) directions. In our model, we assume that the angle corresponding to the maximum anterior CoP position is approximately the most anterior point contained within the foot and maximum plantar flexion torque bounds introduced in constraint C1:

$$\theta_{\text{toeEq}} = \max\left(\theta_{\text{toe}}, \cos^{-1}\left(\frac{\tau_{\text{human}}^{\text{max pf}} - \tau_{\text{exo}}^{\text{sat}}}{mgl}\right)\right) - 0.03. \tag{13}$$

The angle θ_{toeEq} is largest angle such that the model's human and exoskeleton maximum torques, $\tau_{\text{human}}^{\text{max pf}}$ and $\tau_{\text{exo}}^{\text{sat}}$, are sufficient to compensate for gravity and maintain a static position. We subtract 0.03 rad to allow for displacement due to postural sway. When the model torque bounds correspond to a young individual this point occurs at θ_{toe}, but in models of older adults, the region of static support may be smaller. Indeed, in an older adult there may be further limiting factors shrinking the FBOS, such as reduced toe flexor strength [32].

The equilibrium point corresponding to the toe is therefore $x_{\text{toeEq}} = [\theta_{\text{toeEq}}, 0, mgl\cos(\theta_{\text{toeEq}}) - \tau_{\text{exo}}^{\text{sat}}]$. The ankle equilibrium point is more straightforward. We simply let $\theta_{\text{ankEq}} = \frac{\pi}{2}$. This corresponds to upright standing with no forward lean. The ankle equilibrium is $x_{\text{ankEq}} = [\theta_{\text{ank}}, 0, \tau_g - \tau_{\text{exo}}]$, where τ_{exo} is determined by a state feedback law $K_{\text{exo}}(x_1, x_2)$. The ankle and toe equilibria for the system with and without exoskeleton assistance are shown in Figure 3, along with the FBOS. Note that in the no exoskeleton case, we simply set $\tau_{\text{exo}} = \tau_{\text{exo}}^{\text{sat}} = 0$.

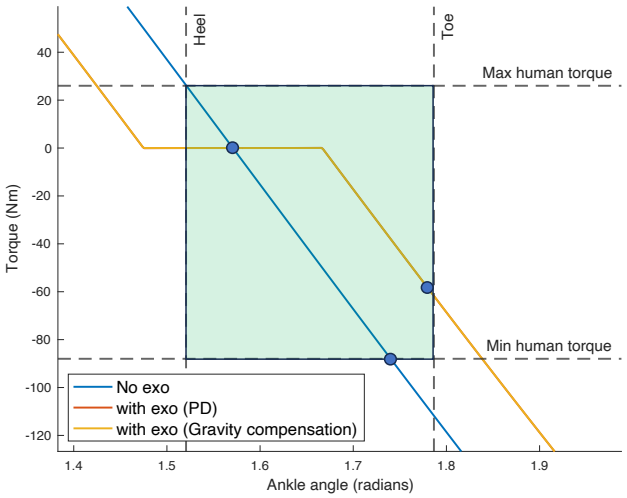

Fig. 3. Continua of equilibrium points in the zero-velocity plane for the system with and without an exoskeleton. The shaded green region indicates the bounds of the foot along the x-axis, and the human torque bounds on the y-axis. The equilibrium point corresponding to the ankle and the points corresponding to the maximum point of static feasible support are marked with blue dots. The bounds in this figure correspond to the older female model.

For a system with a given exoskeleton controller, we linearize the system at each equilibrium point $x_{\text{eq}} \in \{x_{\text{ankleEq}}, x_{\text{toeEq}}\}$ such that we have

$$\dot{\tilde{x}} = A\tilde{x} + B\tilde{u} \tag{14}$$

Where $\tilde{x} = x - x_{\text{eq}}$ is the new state variable representing deviation from x_{eq}. We wish to find some $\tilde{u} = K(\tilde{x})$ that is a closed loop controller guaranteed to stabilize the system about x_{eq}. We can find a CLF of the form $E(\tilde{x}) = \tilde{x}^T P \tilde{x}$ with a corresponding stabilizing controller by solving a semidefinite program, described in Appendix II.

The target set centered at x_{eq} can then be formulated as $\{x \mid (x - x_{\text{eq}})^T P(x - x_{\text{eq}}) \leq c\}$, for some $c \in \mathbb{R}$. However, this CLF is valid for the unconstrained linearized system (14). This means that c should be chosen small enough such that for any x in this ellipsoid, the state and input constraints on the original nonlinear system are satisfied.

To simplify this problem, we first consider only linear constraints. The controller $u = Kx$ should not violate constraint (C2) and the constraint on the human torque production (C1) should also be enforced. Furthermore, the target set should not contain CoM positions anterior or posterior to the foot. As the target set should represent quiet standing, we also add an additional constraint limiting the velocity within the target by an amount close to experimentally observed postural sway [33]. These last two conditions become two additional linear constraints:

$$\theta_{\text{heel}} < x_1 < \theta_{\text{toe}} \tag{C6}$$

$$-v_{\text{sway}} < x_2 < v_{\text{sway}} \tag{C7}$$

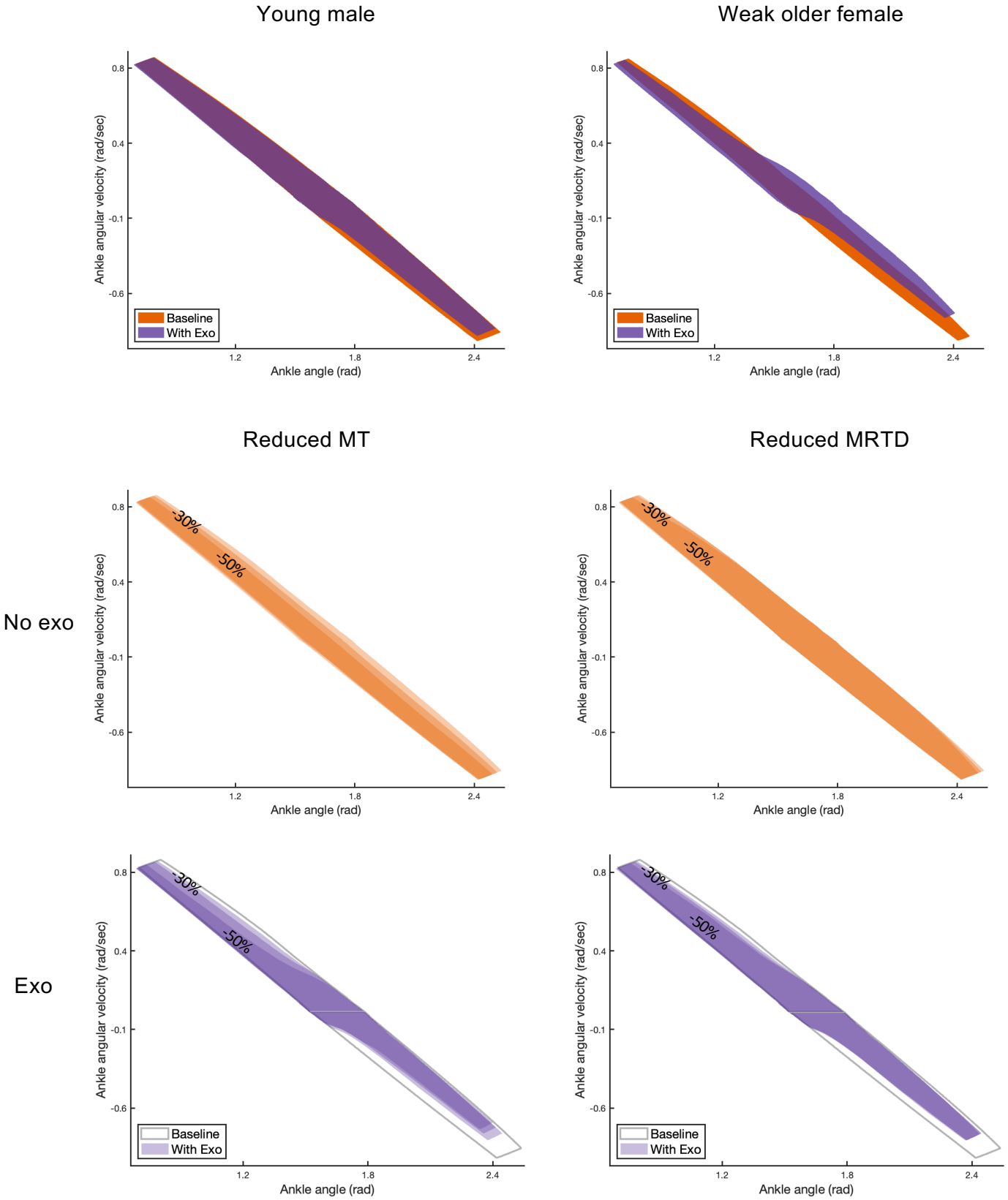

Fig. 4. The top row shows the stabilizable region computed for the young male model (left) and weak older female (right). The baseline regions without the exoskeleton are shown in orange, while the region with exoskeleton assistance is shown in purple. Stabilizable regions when MT and MRTD are reduced independently are shown in the bottom four panels. In the second, the regions are computed with no exoskeleton. The largest sets are baseline, followed by 30% reduction and 50% reduction in each respective quantity. In the bottom row, the exoskeleton is added, and the baseline is outlined in gray.

where v_{sway} represents the maximum allowable postural sway within the target set.

The problem of finding the largest c such that the ellipsoid P is maximally contained within the linear constraints is easy to solve. It is a simplified version of the convex problem of finding a maximum volume inscribed ellipsoid within a polyhedron (see for example [34, Chapter 8]) and has a closed form solution:

$$c = \min_i \frac{(b_i - a_i^T x_{\text{eq}})^2}{a_i^T P^{-1} a_i} \tag{15}$$

Here each of the linear constraints is represented as two inequalities of the form $a_i x \leq b_i$, where $a_i \in \mathbb{R}^{1\times 3}$, $b_i \in \mathbb{R}$, and $i \in \{1, \ldots, 8\}$. A complete derivation is in Appendix II.

For compatibility with the BRS computation tool, we enclose the ellipsoid in a tight axis-aligned bounding box. We check that the vertices are also contained within the constraint polytope. If they are not, we perform a linear search to further scale c such that the constraints are satisfied for the minimum circumscribed axis-aligned bounding box. To account for the nonlinear foot-ground interaction constraints, we check that the box corners do not violate (C3)-(C5). Although this does not provide a provable guarantee of constraint satisfaction, in practice it is a sufficient check due to the relatively small size of the boxes. The target set is then the union of the axis-aligned boxes centered around the ankle and toe equilibria.

C. Evaluating the effect of ankle exoskeleton assistance

To determine how exoskeleton assistance may affect the stability of older adults with differing ankle torque production capabilities, we model five representative individuals. The individuals correspond to the young female (YF), young male (YM), older female (OF), and older male (OM) categories described in [8]. We add the fifth category, weak older female (wOF), by reducing the maximum isometric torque and normalized rate of torque development by half a standard deviation. The respective MT and MRTD bounds of each model are shown in Table I.

For each model, we construct appropriate target sets as described in the previous section, and then use a state of the art HJB toolbox to compute the backward reachable set in position-velocity-torque space [29]. To form the stabilizable region, we project the resulting BRS into position-velocity space. We first compute a baseline stabilizable region for a young male model without exoskeleton assistance, shown in purple for forward velocities in Figure 1. We validate that for a full strength YM model, the bounds approximately coincide with those computed via the XCoM method shown in the same figure in gray. These bounds overlap wherever the model is close to linear.

We then compute the BRS with ankle exoskeleton assistance added. We assume that the motor on each exoskeleton saturates at $25\,\text{N}\cdot\text{m}$ and that each device uses a gravity compensation (GC) control strategy, as described in [19]:

$$K(x) = \begin{cases} mgl\cos\theta & \text{if } |\tau_{\text{exo}}| < \text{motor limit} \\ \pm\text{motor limit} & \text{otherwise,} \end{cases} \tag{16}$$

To understand the effect of damping, we also compute the SR with a proportional derivative controller whose desired setpoint is static, upright standing:

$$K(x) = \begin{cases} K_p(\theta - \frac{\pi}{2}) + K_d(\dot{\theta}) & \text{if } |\tau_{\text{exo}}| < \text{motor limit} \\ \pm\text{motor limit} & \text{otherwise} \end{cases} \tag{17}$$

where $K_p, K_d > 0$ represent the PD controller gains. The gains are also taken from [19], where proportional gain $K_p = mgl$ is a linearized gravity compensation term, while the derivative gain $K_d = 0.3\sqrt{ml^2 K_p}$ compensates for gravitational stiffness. Both the GC and PD controller are easily substituted into the dynamics such that $\tau_{\text{exo}} = K(x)$. While we only analyze these two strategies, we emphasize that the methods presented here can be applied to any state-feedback controller.

To get a clearer picture of the independent contributions of reduced MT and MRTD, we also analyze how reduced MRTD and reduced MT affect the SR separately. We compute the SR for the YF model with the MT held constant at the YF's nominal peak value, while reducing the MRTD in ten percent increments. We repeat this procedure but we reduce the MT while holding the MRTD fixed. We evaluate how deficits in MT and MRTD interact with ankle exoskeleton assistance by computing similarly reduced strength sets with GC exoskeleton assistance added. We compare the area of the reduced strength stabilizable regions with the full strength baseline region, and compute the percent reduction or increase in area.

TABLE I
MODEL PARAMETERS FOR YOUNG FEMALE (YF), OLD FEMALE (OF), YOUNG MALE (YM). OLD MALE (OM), AND WEAK OLDER FEMALE (WOF), INCLUDING MT AND MRTD IN DORSIFLEXION (DF) AND PLANTAR FLEXION (PF) DIRECTIONS

	Dir.	YF	OF	YM	OM	wOF
Mass (kg)	n/a	59.4	60.0	72.9	74.5	60.0
Height (m)	n/a	1.65	1.59	1.77	1.74	1.59
MT (Nm)	DF	28	22	43	37	21
	PF	130	88	181	137	78
MRTD (Nm/sec)	DF	219	148	309	232	130
	PF	608	389	957	681	303

V. RESULTS

A. Stabilizable regions for age and sex adjusted models

Table II summarizes the results for the YF, YM, OM, OF, and wOF models with the gravity compensation (GC) and PD controller strategies. The changes in area for the forward and backward velocity regions are listed separately. In the forward velocity region the GC and PD controller slightly reduce the area of the SR in the young adult models but increase the total area in the OF and wOF model. The backward velocity region shows a different trend — the exoskeleton assistance reduces the area of the stabilizable region for all models. The additional damping provided by the PD controller does not significantly mitigate reductions in stabilizable region area. The stabilizable regions for the young male model and the weak older female model are shown in the top two panels of Figure 4, with and without the exoskeleton added.

v^+	Gravity compensation	Proportional-derivative
YM	−0.43	−0.37
YF	−3.14	−2.73
OM	+3.71	+4.64
OF	+8.43	+9.56
wOF	+15.9	+17.5
v^-	Gravity compensation	Proportional-derivative
YM	−16.9	−16.5
YF	−32.7	−32.4
OM	−15.39	−14.94
OF	−19.56	−18.92
wOF	−10.5	−10.16

TABLE II
EFFECT OF EXOSKELETON ASSISTANCE ON TOTAL AREA OF STABILIZABLE REGION FOR SEX AND AGE ADJUSTED MODELS.

B. Effect of reduced MT and MRTD

The effect of reducing MT and MRTD in 10% increments can been seen in Figure 5 as percent reduction in area relative to the baseline. Figure 4 shows the YF stabilizable region when MT or MRTD are reduced by 30% and 50% with and without exoskeleton assistance. At positive velocities, reducing maximum torque causes large reductions in SR area but the addition of exoskeleton assistance mitigates the overall effect. For example, a 30% MT reduction results in an SR area that is 20% smaller than the baseline region while there is only a 10% reduction when ankle exoskeleton assistance is included. At negative velocities, the shift in the constraints on human torque arising from (4) overpowers any mitigating effect that the exoskeleton assistance my have on reduced MT.

When MRTD is reduced the effect on the overall SR only becomes noticeable after large reductions of 40% or more at positive velocities. When an exoskeleton is added, however, the effect is amplified. Without the exoskeleton a 30% reduction in MRTD causes a 2.6% reduction in SR area. With an exoskeleton the SR area is reduced by 10.4%. At negative velocities, the change in total area is overwhelmingly determined by the change in constraint bounds, as with reduced MT.

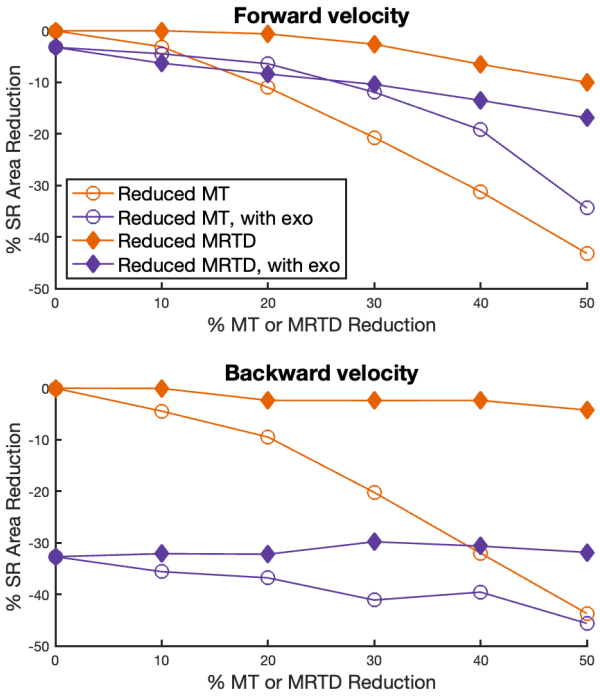

Fig. 5. Trends in stabilizable region area when MT (circular markers) and MRTD (diamond markers) are independently reduced, with (purple) and without the exoskeleton (orange).

VI. Discussion

The stabilizable regions computed without ankle exoskeleton assistance align with what is known from prior experiments in the literature. Reduced MT has a far stronger effect than MRTD, with even a severe reduction in MRTD contributing to only a 10% reduction in total area. Interestingly, the stabilizable regions computed with ankle exoskeleton assistance suggest that the device may exacerbate MRTD deficits. Reductions in MRTD lead to larger reductions in the total stabilizable region area computed with exoskeleton than without. The same effect is not seen for reduced MT, where the ankle exoskeleton seems to mitigate the reduction in area.

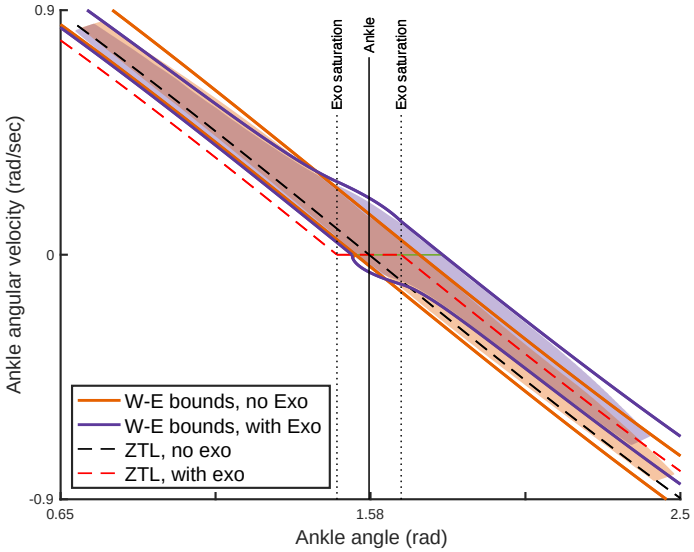

Fig. 6. Boundaries of the SR computed for a simple pendulum using work-energy (W-E) analysis. The regions computed with our method are overlaid in light purple and orange.

However, as can seen clearly in the Figures 4 and 5, the addition of exoskeleton torque does not uniformly increase or decrease the area of the stabilizable region (SR). We see the following effects in the positive (posterior-anterior) velocity region:

- The exo *increases* the SR along the entire backward fall boundary.
- The exo *increases* the SR along the forward fall boundary at low velocities.
- The exo *decreases* the SR along the forward fall boundary at nondimensional velocities higher than approximately 0.2.

At negative (anterior-posterior) velocities we see similar effects:

- The exo *increases* the SR along the forward fall boundary up to nondimensional velocities of approximately -0.7.
- The exo *increases* the SR boundary along the backward fall boundary at low velocities.
- the exo *decreases* the SR along the backward fall boundary at velocities lower than approximately -0.15.
- the exo *decreases* the range of the contact constraint edge (the short edge in the lower right hand corner)

To understand why this may be happening, we will analyze the dynamics of an unconstrained and undamped 2d pendulum, with and without the exoskeleton, e.g. the system with dynamics $\tau_h + \tau_{\text{exo}} = ml^2\ddot{\theta} + mgl\cos(\theta)$.

We first note that gravity exerts a negative torque when the CoM is behind the ankle and a positive torque when the CoM is ahead of the ankle. We can draw a vertical line at $y = \theta_{\text{ankle}}$ that separates the 2d state space into positive and negative gravity torque regions. This is the solid black line shown in Figure 6.

We also need to define a *zero human-torque line*.

Definition 5. The *zero human-torque line (ZTL)* is a line in the phase plane along which the human does not need to produce torque to reach a final static standing condition.

Consider first, the no exoskeleton case — The only static standing position where the human does not need to produce a gravity resisting torque is directly above the ankle. Thus, there is a unique ZTL along which total mechanical energy is a constant, and is equal to the

potential energy when the center of mass is directly above the ankle. If the initial energy is $E_i = mgl\sin\theta + \frac{1}{2}ml^2\dot{\theta}^2$ and the final energy is $E_f = mgl\sin\theta_{\text{ankle}}$ we can compute the zero torque line by letting $E_i = E_f$, and thus derive an equation for the system velocity as a function of position:

$$\dot{\theta} = \pm\sqrt{2\frac{g}{l}(\sin\theta_{\text{ankle}} - \sin\theta)} \tag{18}$$

This is shown as a dashed black line in figure 6.

The ZTL is useful, as it delineates the direction of the optimal human torque. For a trajectory starting below the ZTL, a positive (dorsiflexion) torque must eventually be applied to avoid a backward fall past the heel. For trajectories starting above the zero-torque line, a negative (plantar flexion) torque is eventually necessary to brake quickly enough to prevent the CoM from overshooting past the toe. The boundary of the stabilizable region that is below the ZTL corresponds to the lower bound before a backward fall occurs, whereas the stabilizable region boundary above the ZTL corresponds to forward falls [20].

It is important to note the overlap between the region where dorsiflexion and plantar flexion are required according to the zero torque trajectory, and the direction of the gravitational torque. In large portions of the state space, gravity provides an assistive torque in the optimal direction.

Now let us consider how the addition of an exoskeleton changes the ZTL. For the analysis in this section, we will consider only the case of the gravity compensation exoskeleton. Equation (18) is no longer valid once a gravity compensation torque is added, as the exoskeleton will always apply a torque. To stay on the original ZTL, i.e. the ZTL without an exoskeleton, the human would have to produce a torque resisting the exoskeleton.

Recall that the exoskeleton torque saturates at a negative and positive value. In the case of the gravity compensation controller we can easily calculate the angles at which the postive and negative saturations occur. We can therefore divide the state space into three regions: with positive saturation, where $\tau_{\text{exo}} = \tau_{\text{sat}}$; no saturation, where $\tau_{\text{exo}} = mgl\cos\theta$; and negative saturation,where $\tau_{\text{exo}} = -\tau_{\text{sat}}$. The ZTL must be computed for each of these regions in a piecewise manner.

In the region where the controller is not saturated, the exoskeleton torque fully compensates for the gravitational torque, meaning that the human must generate no additional torque along this range of angles. The endpoints of this range are where the exoskeleton saturation torque can fully compensate for gravity without additional torque from the human. Denoting these angles as $\theta^{\text{ub}}_{\text{sat}}$ and $\theta^{\text{lb}}_{\text{sat}}$, the ZTL can be derived using the work-energy principle, similar to (18) but with the addition of the work due to the saturated exoskeleton. For example,

$$\dot{\theta} = \sqrt{2(\tau^{\text{sat}}_{\text{exo}}(\theta^{\text{ub}}_{\text{sat}} - \theta) + \frac{g}{l}(\sin\theta^{\text{ub}}_{\text{sat}} - \sin\theta))} \tag{19}$$

is the ZTL in the region of positive exoskeleton saturation. The full ZTL with exoskeleton assistance is shown in Figure 6 as a dashed red line.

Examining the ZTL with the exoskeleton actuation we can see that in the forward velocity half of the phase plane the line is shifted to the left, such that a plantar flexion braking torque is always required to prevent forward falls. Interestingly, the addition of the exoskeleton effectively eliminates the possibility of a backward fall occurring, as long as there is an initial positive velocity and the contact constraints are satisfied. In the negative velocity half of the plane the ZTL is shifted to the right, increasing the area where a dorsiflexion braking torque is needed to prevent a backward fall. Recalling that the maximum dorsiflexion torque magnitude can be as low as 25% of maximum plantar flexion torque it is not surprising that the increased reliance on dorsiflexion also causes the constraint failure edge to shift inward. These shifts in the ZTL mean that the exoskeleton qualitatively changes the optimal human response required to stabilize to quiet standing in large regions of the state space.

As noted earlier, gravity sometimes provides an assistive torque in the no exoskeleton case. Therefore, if the exoskeleton controller is designed to cancel the gravitational torque, we might expect that exoskeleton "assistance" does not uniformly improve stability. On the other hand, the exoskeleton increases the torque bounds of the human user. This is particularly notable in weaker models as foot-ground interaction constraints are the main limiting factor for stronger models. In particular, static stability is increased in weaker models, resulting in a larger functional base of support.

There is therefore a trade-off which we can think of in terms of work. A weak adult wearing the exoskeleton has the ability to do more work, but they must compensate at times for the gravitational torque being canceled out. We can use the work-energy principle to delineate how this tradeoff affects stabilizability.

The net work of the system is the sum of the work done by the human, exoskeleton, and gravity. Note that the net work done by gravity and the exoskeleton will always have opposite signs due to the controller formulation. For most initial conditions reaching the target set requires a reduction in kinetic energy, i.e. negative work,

$$-ml^2\dot{\theta}_i^2 = \int_{\theta_i}^{\theta_f}(\tau_{\text{exo}} + \tau_{\text{gravity}} + \tau_{\text{human}})d\theta. \tag{20}$$

By selecting an appropriate final position θ_f, and by assuming that the human produces a constant optimal torque, upper and lower boundaries on the stabilizable region can be computed in a piecewise manner on the position-velocity plane. For example, for $\theta_i < \theta^{\text{lb}}_{\text{sat}}$ the upper boundary is expressed by the relation

$$\begin{aligned}-ml^2\dot{\theta}_i^2 =& \tau^{\text{sat}}_{\text{exo}}(\theta^{\text{lb}}_{\text{sat}} - \theta) + (-mgl)(\sin\Big(\theta^{\text{lb}}_{\text{sat}}\Big) - \sin(\theta)) + \\ & \tau^{\text{max pf}}_{\text{human}} \cdot (\theta^{\text{lb}}_{\text{sat}} - \theta) + (-mgl)(\sin\Big(\theta^{\text{ub}}_{\text{sat}}\Big) - \sin\big(\theta_{\text{toeEq}}\big)) + \\ & mgl\cos\big(\theta_{\text{toeEq}}\big)(\theta^{\text{ub}}_{\text{sat}} - \theta_{\text{toeEq}}).\end{aligned} \tag{21}$$

The bounds derived from the work-energy analysis are shown for the system with (purple) and without (orange) the gravity compensating exoskeleton in Figure 6. As can be seen in the figure, the computed BRS for the exo and non-exo systems are well-approximated by these bounds, demonstrating that the changes in the stabilizable region boundaries can be understood from a work-energy perspective. This analysis, however, assumes conservation of energy and ignores contact and input constraints, leading to an overestimation of the true boundaries. Additionally, it cannot generalize to systems with dissipation — such as exoskeleton controllers with damping.

The stabilizable regions computed with our reachability analysis can therefore increase within these work-energy bounds, subject to foot-ground contact and MRTD constraints. The lack of any significant reduction in area in the full-strength YM model is the result of having a large enough range of positive and negative maximum torque and a large enough MRTD such that the exoskeleton's undesirable behavior can be compensated for quickly. An exoskeleton that can completely compensate for missing MT and MRTD and uses proportional myo-electric control could lead to similar outcomes.

To enable analysis of myo-electric controllers, we will include more detailed muscle actuation models in our future work. We will also model delay and relax our assumption that the human adapts optimally to the exoskeleton assistance. The results presented here

can also serve as a guide in the design of perturbation experiments of older adults wearing exoskeletons.

APPENDIX I
DERIVATION OF EQUATIONS OF MOTION AND CONSTRAINTS

Here we derive the equations of motion and state constraints presented in Section III.

A. Equations of Motion

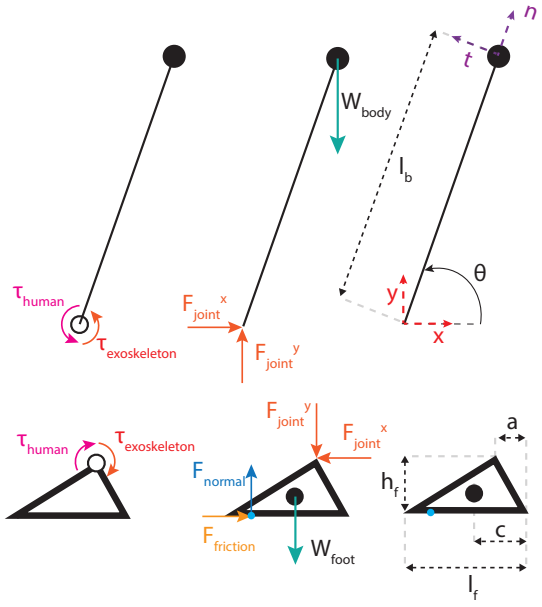

Fig. 7. Free body diagram of system

A free body diagram of the system is shown in Figure 7. To derive the constraints that prevent the foot from slipping or tipping, we must first understand what torques and forces are acting on the foot.

In the following, we will denote $\cos(\theta)$ as c_θ and $\sin(\theta)$ as s_θ for particularly unwieldy equations. Let $\tau = \tau_{\text{human}} + \tau_{\text{exoskeleton}}$ be the total internal torque at the ankle. Summing the torques for the body segment at the ankle, we have

$$\tau = ml_b^2\ddot{\theta} + mgl_b\cos\theta, \tag{22}$$

where ml_b^2 is the moment of inertia of the body segment. The rotational motion of the body segment can be decomposed into a normal acceleration along the leg

$$a^n = -l_b\dot{\theta}^2 \tag{23}$$

and a tangential acceleration

$$a^t = l_b\ddot{\theta}. \tag{24}$$

Rotating these accelerations to the x-y coordinate system, we have -

$$a^x = a^n c_\theta - a^t s_\theta = -l_b(\dot{\theta}^2 c_\theta + \ddot{\theta}s_\theta) \tag{25}$$

$$a^y = a^n s_\theta + a^t c_\theta = l_b(-\dot{\theta}^2 s_\theta + \ddot{\theta}c_\theta) \tag{26}$$

These accelerations are caused by a combination of the weight of the body and the contact forces at the ankle joint. Thus we can write the force balance at the ankle as:

$$ma^x = F^x_{\text{joint}} = -ml_b(\dot{\theta}^2 c_\theta + \ddot{\theta}s_\theta) \tag{27}$$

$$ma^y = F^y_{\text{joint}} - W_{\text{body}} = F^y_{\text{joint}} - mg = ml_b(-\dot{\theta}^2 s_\theta + \ddot{\theta}c_\theta) \tag{28}$$

Similarly, for the foot segment we can write the force balance as:

$$m_f a^x_f = F_{\text{friction}} - F^x_{\text{joint}} \tag{29}$$

$$m_f a^y_f = F_{\text{normal}} - F^y_{\text{joint}} - W_{\text{foot}} = F_{\text{normal}} - F^y_{\text{joint}} - m_f g \tag{30}$$

where m_f is the mass of the foot. When the foot is not accelerating we get:

$$F_{\text{normal}} = F^y_{\text{joint}} + m_f g \tag{31}$$

This gives us an equation for F_{normal}:

$$F_{\text{normal}} = ml_b(-\dot{\theta}^2 s_\theta + \ddot{\theta}c_\theta) + mg + m_f g \tag{32}$$

Similarly, we can derive an expression for the ground reaction/friction force in the x direction via force balancing:

$$F_{\text{friction}} = F^x_{\text{joint}} = -ml_b(\dot{\theta}^2 c_\theta + \ddot{\theta}s_\theta) \tag{33}$$

Finally, the location of the center of pressure (CoP) as a function of these known quantities can be found by balancing torques about the ankle:

$$((l_f - a) - \text{CoP}) \cdot F_{\text{normal}} - cm_f g + \tau - h_f F_{\text{friction}} = 0 \tag{34}$$

which in turn gives us

$$\text{CoP} = (l_f - a) - \frac{cm_f g - \tau + h_f F_{\text{friction}}}{F_{\text{normal}}} \tag{35}$$

B. State Constraints

Constraints C3 and C5 can be converted into state constraints on τ by first solving 22 for the acceleration:

$$\ddot{\theta} = \frac{1}{ml_b^2}\tau - \frac{g}{l_b}c_\theta \tag{36}$$

For Constraint C3, substituting for $\ddot{\theta}$ into (32) gives us

$$ml(-\dot{\theta}^2 s_\theta + (\frac{1}{ml^2}\tau - \frac{g}{l}c_\theta)c_\theta) + mg + m_f g \geq 0. \tag{37}$$

Solving for τ, after some algebra we see that

$$\tau \geq \frac{-l(m+m_f)g + ml^2\dot{\theta}^2 s_\theta}{c_\theta} + mglc_\theta \tag{38}$$

if $c_\theta > 0$, with the direction of the inequality flipped if $c_\theta < 0$.

Similarly, plugging (36) into Constraint C5 results in four inequalities constraining τ. Letting $\rho_1 = \mu c_\theta + s_\theta$ and $\rho_2 = \mu c_\theta + s_\theta$, when $\rho_1 < 0$

$$\tau < mglc_\theta + \frac{(\mu s_\theta - c_\theta)ml^2\dot{\theta}^2 - \mu lg(m_f + m)}{\rho_1} \tag{39}$$

with the direction of the inequality flipped when $\rho_1 > 0$. When $\rho_2 < 0$,

$$\tau < mglc_\theta + \frac{(\mu s_\theta + c_\theta)ml^2\dot{\theta}^2 - \mu lg(m_f + m)}{\rho_2} \tag{40}$$

Lastly, constraints on τ are derived from C4 by first incorporating the parameters of the foot:

$$0 \leq \text{CoP} \leq l_f \tag{41}$$

Plugging in our expression for the CoP, equation (35), gives us two corresponding inequalities:

$$\tau < aF_{\text{normal}} + h_f F_{\text{friction}} + cm_f g \tag{42}$$

and

$$\tau > -(l_f - a)F_{\text{normal}} + cm_f g + h_f F_{\text{friction}} \tag{43}$$

APPENDIX II
TARGET SET COMPUTATION

A. Computing the CLF

we can write the following optimization problem, where both constraints come from Definition 4:

$$\begin{aligned} \min_{P,K} \quad & \mathrm{Tr}(P) \\ \text{s.t.} \quad & P > 0 \\ & (A+BK)^T P + P(A+BK) < 0 \end{aligned} \tag{44}$$

This problem is nonlinear in K and P, but it can be converted to a convex SDP. First, we multiply the second constraint by P^{-1} on both sides, so that it becomes

$$P^{-1}((A+BK)^T + (A+BK))P^{-1} < 0. \tag{45}$$

Letting $Q = P^{-1}$ and $Y = KQ$, we can now write an SDP with linear constraints

$$\begin{aligned} \min_{Q,Y} \quad & \mathrm{Tr}(Q) \\ \text{s.t.} \quad & Y^T B^T + QA^T + BY < 0. \end{aligned} \tag{46}$$

We now have a CLF $E(x) = x^T P x$, where $P = Q^{-1}$, and a controller $u = Kx$, where $K = YP$.

B. Computing maximally scaled ellipsoids

Let $(x - x_{\text{eq}})^T P (x - x_{\text{eq}})$ be the CLF corresponding to a given equilibrium point. Let $A_{\text{con}} x = b_{\text{con}}$ represent a set of n linear constraints. We wish to find the largest c such that the ellipsoid $\mathcal{E} = \{x | (x - x_{\text{eq}})^T P (x - x_{\text{eq}}) \leq c\}$ is fully contained within the constraints. Denote a_i, b_i the ith row of A_{con} and entry of b_{con}, respectively. In the case of a single constraint hyperplane $a_i^T x \leq b_i$, it is clear that the largest possible c should produce an ellipsoid that just touches the constraint at one point. This can be cast as a simple convex optimization problem:

$$\begin{aligned} \min_{x} \quad & (x - x_{\text{eq}})^T P (x - x_{\text{eq}}) \\ \text{s.t.} \quad & a_i^T x = b_i \end{aligned} \tag{47}$$

By the method of Lagrange multipliers, we have that the Lagrangian $L(x) = (x - x_{\text{eq}})^T P (x - x_{\text{eq}}) + \lambda(a_i^T x - b_i)$. Taking the partial derivatives, we solve

$$\begin{aligned} 2P(x - x_{\text{eq}}) + \lambda a_i^T &= 0, \\ a_i^T x - b_i &= 0 \end{aligned} \tag{48}$$

for λ, x. After some algebra this gives an expression for c, which in turn should be minimized over all n constraints:

$$c = \min_i \frac{(b_i - a_i^T x_{\text{eq}})^2}{a_i^T P^{-1} a_i} \tag{49}$$

APPENDIX III
COMPUTATIONAL CONSIDERATIONS

To improve computational performance, the states of system (3) were nondimensionalized. Angular velocities $\dot{\theta}$ were scaled by $\omega = \sqrt{l/g}$, the natural frequency of the pendulum. The human torque state τ_h was nondimensionalized by multiplying by $\frac{\omega^2}{ml^2}$.

The backward reachable set was computed in the nondimensionalized state space over a $225 \times 225 \times 225$ grid. This was the coarsest grid which produced sufficiently clean results. We found that results computed over coarser grids were too noisy.

ACKNOWLEDGMENT

Thanks to Anat Raman for the many fruitful discussions.

REFERENCES

[1] K. L. Poggensee and S. H. Collins, "How adaptation, training, and customization contribute to benefits from exoskeleton assistance," *Science Robotics*, vol. 6, no. 58, p. eabf1078, 2021.
[2] A. Lakmazaheri, S. Song, B. B. Vuong, B. Biskner, D. M. Kado, and S. H. Collins, "Optimizing exoskeleton assistance to improve walking speed and energy economy for older adults," *Journal of NeuroEngineering and Rehabilitation*, vol. 21, no. 1, p. 1, 2024.
[3] M. Raitor, S. W. Ruggles, S. L. Delp, C. K. Liu, and S. H. Collins, "Lower-limb exoskeletons appeal to both clinicians and older adults, especially for fall prevention and joint pain reduction," *IEEE Transactions on Neural Systems and Rehabilitation Engineering*, vol. 32, pp. 1577–1585, 2024.
[4] F. B. Horak and L. M. Nashner, "Central programming of postural movements: adaptation to altered support-surface configurations," *Journal of neurophysiology*, vol. 55, no. 6, pp. 1369–1381, 1986.
[5] C. J. Hasson, R. E. van Emmerik, and G. E. Caldwell, "Balance decrements are associated with age-related muscle property changes," *Journal of Applied Biomechanics*, vol. 30, no. 4, pp. 555 – 562, 2014.
[6] T. Cattagni, G. Scaglioni, D. Laroche, J. Van Hoecke, V. Gremeaux, and A. Martin, "Ankle muscle strength discriminates fallers from non-fallers," *Frontiers in Aging Neuroscience*, vol. 6, 2014.
[7] T. Cattagni, G. Scaglioni, D. Laroche, V. Gremeaux, and A. Martin, "The involvement of ankle muscles in maintaining balance in the upright posture is higher in elderly fallers," *Experimental Gerontology*, vol. 77, pp. 38–45, 2016.
[8] D. G. Thelen, A. B. Schultz, N. B. Alexander, and J. A. Ashton-Miller, "Effects of Age on Rapid Ankle Torque Development," *The Journals of Gerontology: Series A*, vol. 51A, pp. M226–M232, 09 1996.
[9] P. C. B. Bento, G. Pereira, C. Ugrinowitsch, and A. L. F. Rodacki, "Peak torque and rate of torque development in elderly with and without fall history," *Clinical biomechanics*, vol. 25, no. 5, pp. 450–454, 2010.
[10] T. Kamo, R. Asahi, M. Azami, H. Ogihara, T. Ikeda, K. Suzuki, and Y. Nishida, "Rate of torque development and the risk of falls among community dwelling older adults in japan," *Gait & Posture*, vol. 72, pp. 28–33, 2019.
[11] R. Ema, M. Saito, S. Ohki, H. Takayama, Y. Yamada, and R. Akagi, "Association between rapid force production by the plantar flexors and balance performance in elderly men and women," *Age*, vol. 38, pp. 475–483, 2016.
[12] D. P. LaRoche, K. A. Cremin, B. Greenleaf, and R. V. Croce, "Rapid torque development in older female fallers and nonfallers: a comparison across lower-extremity muscles," *Journal of electromyography and kinesiology*, vol. 20, no. 3, pp. 482–488, 2010.
[13] M. Pijnappels, J. Van der Burg, N. D. Reeves, and J. H. van Dieën, "Identification of elderly fallers by muscle strength measures," *European journal of applied physiology*, vol. 102, pp. 585–592, 2008.
[14] O. N. Beck, M. K. Shepherd, R. Rastogi, G. Martino, L. H. Ting, and G. S. Sawicki, "Exoskeletons need to react faster than physiological responses to improve standing balance," *Science Robotics*, vol. 8, no. 75, p. eadf1080, 2023.
[15] S. Sharafi and T. K. Uchida, "Stability of human balance during quiet stance with physiological and exoskeleton time delays," *IEEE Robotics and Automation Letters*, vol. 8, no. 10, pp. 6211–6218, 2023.
[16] N. Rao and A. S. Aruin, "Automatic postural responses in individuals with peripheral neuropathy and ankle–foot orthoses," *Diabetes Research and Clinical Practice*, vol. 74, no. 1, pp. 48–56, 2006.
[17] S. Canete, E. B. Wilson, W. G. Wright, and D. A. Jacobs, "The effects of exoskeleton assistance at the ankle on sensory integration during standing balance," *IEEE Transactions on Neural Systems and Rehabilitation Engineering*, vol. 31, pp. 4428–4438, 2023.
[18] J. Son and J. Ashton-Miller, "Do ankle orthoses improve ankle proprioceptive thresholds or unipedal balance in older persons with peripheral neuropathy?," *American Journal of Physical Medicine and Rehabilitation*, vol. 89, no. 5, pp. 369–375, 2010.
[19] A. R. Emmens, E. H. F. van Asseldonk, and H. van der Kooij, "Effects of a powered ankle-foot orthosis on perturbed standing balance," *Journal of NeuroEngineering and Rehabilitation*, vol. 15, no. 1, p. 50, 2018.
[20] Y.-C. Pai and J. Patton, "Center of mass velocity position predictions for balance control," *Journal of Biomechanics*, vol. 30, no. 4, pp. 347 – 354, 1997.

[21] F. Yang, D. Espy, and Y.-C. Pai, "Feasible stability region in the frontal plane during human gait," *Annals of biomedical engineering*, vol. 37, pp. 2606–2614, 2009.
[22] H. Bahari, J. Forero, J. C. Hall, J. S. Hebert, A. H. Vette, and H. Rouhani, "Use of the extended feasible stability region for assessing stability of perturbed walking," *Scientific Reports*, vol. 11, no. 1, p. 1026, 2021.
[23] A. Hof, M. Gazendam, and W. Sinke, "The condition for dynamic stability," *Journal of Biomechanics*, vol. 38, no. 1, pp. 1–8, 2005.
[24] C. Mummolo, L. Mangialardi, and J. H. Kim, "Numerical estimation of balanced and falling states for constrained legged systems," *Journal of Nonlinear Science*, vol. 27, pp. 1291–1323, 2017.
[25] R. Orsolino, M. Focchi, S. Caron, G. Raiola, V. Barasuol, D. G. Caldwell, and C. Semini, "Feasible region: An actuation-aware extension of the support region," *IEEE Transactions on Robotics*, vol. 36, no. 4, pp. 1239–1255, 2020.
[26] K. A. Inkol and J. McPhee, "Using dynamic simulations to estimate the feasible stability region of feet-in-place balance recovery for lower-limb exoskeleton users," in *2022 9th IEEE RAS/EMBS International Conference for Biomedical Robotics and Biomechatronics (BioRob)*, pp. 1–6, 2022.
[27] D. Raz, L. Yang, B. R. Umberger, and N. Ozay, "Determining the domain of stable human sit-to-stand motions via controlled invariant sets and backward reachability," in *2023 European Control Conference (ECC)*, pp. 1–7, 2023.
[28] M. Vukobratović and B. Borovac, "Zero-moment point—thirty five years of its life," *International journal of humanoid robotics*, vol. 1, no. 01, pp. 157–173, 2004.
[29] I. Mitchell, A. Bayen, and C. Tomlin, "A time-dependent hamilton-jacobi formulation of reachable sets for continuous dynamic games," *IEEE Transactions on Automatic Control*, vol. 50, no. 7, pp. 947–957, 2005.
[30] M. Chen and C. J. Tomlin, "Hamilton–jacobi reachability: Some recent theoretical advances and applications in unmanned airspace management," *Annual Review of Control, Robotics, and Autonomous Systems*, vol. 1, no. 1, pp. 333–358, 2018.
[31] E. D. Sontag, "A lyapunov-like characterization of asymptotic controllability," *SIAM journal on control and optimization*, vol. 21, no. 3, pp. 462–471, 1983.
[32] M. Endo, J. A. Ashton-Miller, and N. B. Alexander, "Effects of Age and Gender on Toe Flexor Muscle Strength," *The Journals of Gerontology: Series A*, vol. 57, pp. M392–M397, 06 2002.
[33] P. Era, P. Sainio, S. Koskinen, P. Haavisto, M. Vaara, and A. Aromaa, "Postural Balance in a Random Sample of 7,979 Subjects Aged 30 Years and Over," *Gerontology*, vol. 52, pp. 204–213, 07 2006.
[34] S. Boyd and L. Vandenberghe, *Convex Optimization*. Cambridge University Press, 2004.